TEST Engineering & Management

July – August 2020
ISSN: 0193-4120 Page No. 3608 - 3615

Active Stereovision based Real-time Detection of Deformation on a Rotating Wind Turbine Blade

Xiaobin Lin[1], Chen Lin[1]*

1. Department of Physics and Electronic Information, Minjiang University, Fuzhou 350108, China
Corresponding Author's Email: linchen1988@foxmail.com

Article Info
Volume 83
Page Number: 3608 - 3615
Publication Issue:
July - August 2020

Article History
Article Received*: 06 June 2020*
Revised*: 29 June 2020*
Accepted*: 14 July 2020*
Publication*: 25 July 2020*

Abstract: In order to detect the deformations on a rotating wind turbine blade, a real-time deformation detection method based on active stereovision is proposed. It casts laser pattern on the target blade in the bright outdoor ambient light condition to improve the performance of stereo matching. The light pattern is also used to help distinguish the foreground and background objects. The fast sum of absolute difference criterion is adopted for quick stereo matching. Then the combination of epipolar constraint, the uniqueness constraint, the ordering constraint, the continuity constraint, and the disparity range constraint is applied in the process of disparity optimization. Subsequently the reference plane is generated by surface fitting based on the point cloud aquired. At last the 3D points with abrupted depth changes compared with the reference plane are deemed as the deformation area and the width and depth of this area are calculated. Experiment results indicate that the proposed method is efficient and reliable in the real-time detection of deformation on an operating wind turbine blade.

Keywords: wind turbine blades; deformation detection; real-time detection; structural health monitoring; active stereovision

1. Introduction

Wind turbines create pollution-free and cost-effective clean energy for many wind-powered thermal systems. Being the most important component of wind turbines, the design and reliability of blades largely determine the performance of power generation[1-4]. Wind turbine blades (WTBs) are usually made of carbon fiber reinforced polymer (CFRP) and glass fiber reinforced polymer (GFRP). Despite of the toughness of these composite materials, these blades are still predisposed to different forms of damages such as aging, abrasion, and cracking owing to the effects of adverse weather during their long-time exposure in outdoor environment. These damages have a significant impact on the cost control and output efficiency of wind power, and may lead to major accidents causing personal injury [5-7]. Currently offline inspection is the main method for the detection of WTB damages, which can only be implemented on halted wind turbines. Wind turbines are mostly halted due to faults. Therefore, offline inspection is unsuitable for dynamic monitoring and prewarning of blade damages.

Online detection for WTBs can timely and effectively detect blade damages, reduce blade maintenance costs, and prevent the occurrence of major accidents[8,9]. Therefore, many researchers have attempted to develop effective SHM (Structural Health Monitoring) methods by various technical means including vibration-based detection, acoustic emission detection, fiber-optic sensors, machine vision inspection technology, and thermal infrared imaging[10-15]. Among these non-destructive damage detection methods, machine vision inspection has gradually emerged as a promising one due to its non-contact and high measurement speed feature, full-field measurement capacity, and the ability to acquire additional information[15,16].

In this research, a fast 3D shape reconstruction method based on active stereovision is proposed to

July – August 2020
ISSN: 0193-4120 Page No. 3608 - 3615

detect the deformation of rotating WTBs in real time. In order to maximally eliminate the impact of blade rotation, the proposed method introduces dual high-speed cameras and short exposure time to resolve ambiguity in the process of image acqusition. Active projection of laser pattern is adopted for efficient and reliable stereo matching, as well as segmentation of foreground object, namely the target WTB, in the outdoor environment. The deformation area is detected and measured by the comparison of the reference plane, which is generated via surface fitting based on the majority of point cloud representing the target blade, and the 3D points with abrupt depth changes which represents the deformed area.

The main contributions of the work is that it proposes and verifies a framework for dynamic detection and measurement of the deformation on rotating WTBs. The combination of high-speed cameras, laser projection device, and the constraints in disparity optimization collectively contribute to the dynamic detection and measurement of deformations.

2. Stereovision model

The principle of stereovision is similar to the stereoscopic view of human vision, which utilizes the disparity in a sequence of 2D images taken from two different locations and perspectives to recover the 3D information of the target object[17]. According to the placement of cameras, the stereovision system model can be divided into two types: parallel stereovision model and convergence stereovision model. These two types of stereovision models have different spatial geometric systems and hence different spatial coordinate calculation methods.

In this work, the parallel stereovision model was adopted due to that it bypasses vertical disparity to result in reduced complexity in 3D coordinate recovery. As illustrated in Figure 1, the target point P in the space projects two image points on the two parallel cameras located on the same plane, respectively Pl on the left camera Cl and Pr on the right camera Cr. Due to the complete overlapping of the two image planes and the parallelism of the two optical axes, the two homologous image points Pl and Pr would have same vertical coordinate value but different horizontal coordinate value, i.e., Yl=Yr, Xl≠Xr. On the condition that the baseline length and focal length are known, the 3D coordinates of target point P could be computed basing on Xl-Xr, namely horizontal disparity.

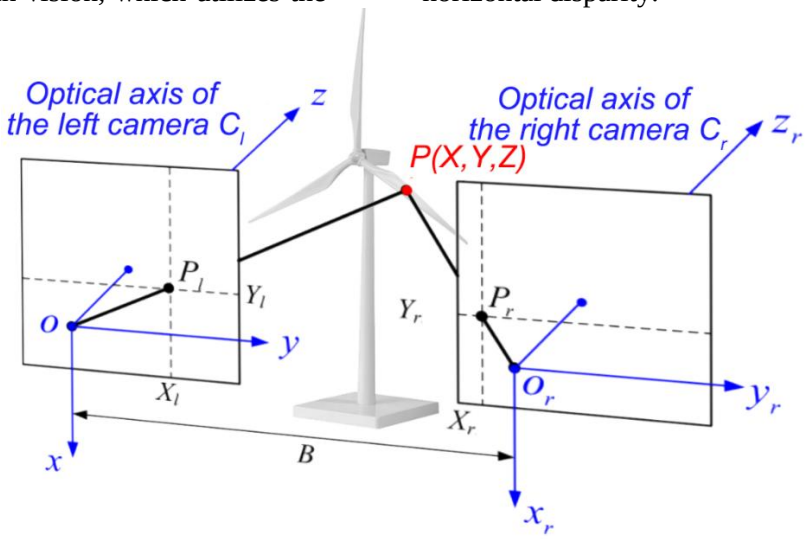

Figure .1 Principle of stereovision.

Let B denote the length of baseline, i.e., the distance between the optical centers of the two cameras, and f denote the focal length, the 3D coordinates X, Y, and Z of target point P can be obtained as follows

$$\begin{cases} Y = \dfrac{B \times Y_l (or\ Y_r)}{v_l - v_r} \end{cases} \quad (1)$$

In the above ideal parallel stereovision model shown in Figure 1., the homologous points Pl and Pr are on the same raster line hence a simple 1D search would easily reveal the position of matching point given the coordinates of one point. However, the vertical disparity is usually inevitable in the stereo images obtained in real-life cases due to the assembling and imaging errors of the two cameras. Therefore, epipolar rectification was introduced in this work to transform the stereo image planes so that each pair of stereo images would have their conjugate epipolar lines collinear. The important advantage of rectification is that the search scope of stereo correspondences is reduced from a 2D plane to a 1D line.

July – August 2020
ISSN: 0193-4120 Page No. 3608 - 3615

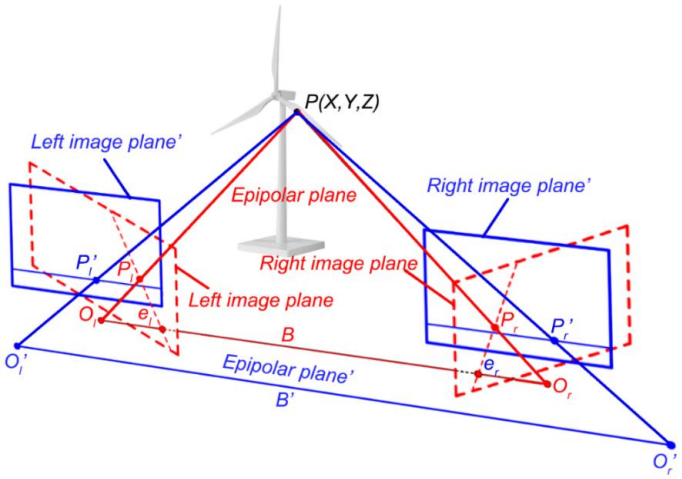

Figure. 2 Principle of epipolar rectification.

Figure 2 shows the change before epipolar rectification (denoted in red color) and after epiploar rectification (denoted in blue color). It should be noted that the intrinsic and extrinsic parameters of two cameras obtained by Zhang's calibration method[18] prior to epiploar rectification are also adjusted with epipolar rectification. The original effective focal lengths of two cameras, namely fl and fr in the intrinsic matrices As, are adjusted to have a same value f. The y-component and z-component in the translation matrix T are reset to zeros, which leaves the baseline B the only non-zero component in the matrix. Unitl now, given the matching points Pl on the left image and Pr on the right camera are identified, the B, f, and horizontal disparity in the equation (1) are all known, whereby the 3D coordinates of target point P can then be computed. While the deformation information can be obtained via the measurement of the point sets forming the deformed surface.

3. Stereo matching

Active stereo matching, which projects coded structured light patterns onto objects to create additional matching features so as to reduce the complexity of stereo matching, was adopted in this work. The introduction of structured light not only improves the performance of stereo match, it also contributes to the distinguishment between the WTB and background. In order to create visible light patterns under the possible strong ambient illumination conditions, a 11 × 11 dot matrix projected by laser was selected in this work as the light pattern. This light pattern projected onto the WTB creates additional feature on the textureless blades which contributes to easier matching of corresponding areas on two images and simpler separation of the WTB and background.

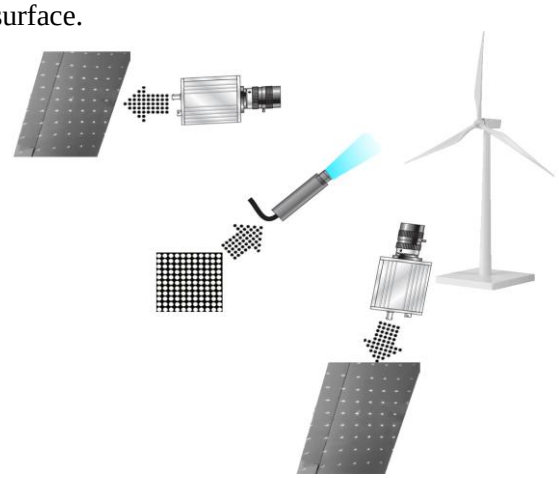

Figure. 3 Schematic diagram of the active stereovision system used in this work.

The unevenly distributed and sparse disparity map obtained via feature matching can only yield sparse 3D point clouds rather than dense 3D point clouds. Therefore, area matching was adopted in this work. There groups of window size, respectively 7×7,13×13, and 19×19, were analyzed with the Tsukuba pair from the Middlebury stereo evaluation dataset to determine the best window size for stereo

July – August 2020
ISSN: 0193-4120 Page No. 3608 - 3615

matching in this work. The generated disparity map suggests the smallest 7 × 7 window result in discontinued and broken disparity map, while the largest 19×19 window result in blurry edges and details. After comprehensive comparison, the medium window size of 13×13 was adopted in the research.

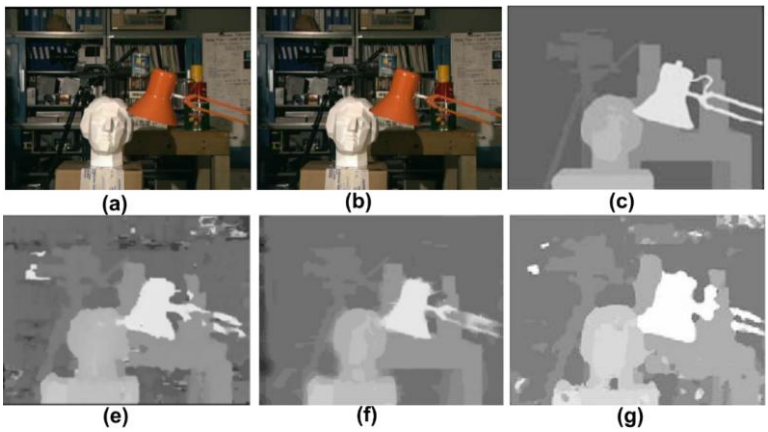

Figure. 4 Disparity map based on different window size: (a) left Tsukuba image; (b) right Tsukuba image; (c) true disparity map; (d) disparity map with window size 7×7; (e) disparity map with window size 13×13; (f) disparity map with window size 19×19.

There are many well-established correlation criteria for area matching such as sum of absolute difference (SAD)[19,20], sum of squared difference (SSD) [20], normalized crosscorrelation (NCC)[20,21], zero mean normalized cross correlation (ZNCC)[20]. NCC and ZNCC have higher accuracy when compared with SAD and SSD, meanwhile, the higher computational complexities have made them unsuitable for real-time applications[22]. Considering the real-time constraint and that the actively projected light pattern would provide more feature for better matching, the fastest SAD was chosen in this work. The SAD correlation criterion is given as follows

$$SAD = \sum_{y=1}^{N} \sum_{x=1}^{M} |f(x,y) - g(x,y)| \quad (2)$$

where f(x,y) is the gray value of the reference image subset, g(x,y) is the gray value of the search image subset, M is the number of horizontal pixels in the image subset, and N is the number of vertical pixels in the image subset. The smaller the value of SAD is, the higher correlation the two image subsets have.

4. Optimization of disparity

The initial homologous point set can be computed once the correlation criterion and window size of area matching are determined, whereafter the initial disparity map of the two images can be obtained. In order to eliminate the ambiguity in this step, i.e. identify the ture matching point given a number of points with similar correlation value, researchers have suggested numerous constraints including the epipolar constraint, the uniqueness constraint, the ordering constraint, the continuity constraint, and the disparity range constraint.

The epipolar constraint excludes false matches between points on different epipolar lines on the rectified stereo image pairs. The uniqueness constraint constrains that every pixel in one stereo image has exactly one matching pixel in the other image, or no matching pixel at all in the case of partial occlusion. This constrain may not hold for scenes with transparent or semi-transparent surfaces. Relate to this work, the uniqueness constraint was realized by only retaining the pixel with the minimum SAD as the matching point. The ordering constraint stipulates that the points and their matching points in the conjugate epipolar lines in the stereo image pairs should appear in the same order. The continuity constraint assumes that the observed surfaces are smooth and continuous apart from object boundaries, therefore the disparity should vary within a certain range and the corresponding Probability Distribution Histogram (PDH) should mostly concentrate within some continuous interval. The disparity range constraint imposes the upper and lower threshholds to exclude false matches, i.e. [Dmin, Dmax].

The aforementioned 5 constraints were adopted in combination to optimize the disparity map in this work. The detailed optimization steps are listed as below.

(1) Segmenting the WTB in the stereo image pairs.

Benefiting from the light pattern projected onto the WTB, the blade area can be segmented for imposing more precise disparity continuity and range constraints. Considering the matrix structure of the light pattern, Hough line transformation limted to 0

July – August 2020
ISSN: 0193-4120 Page No. 3608 - 3615

and $\frac{\pi}{2}$ radian degrees, i.e. computing only horizontal and vertical Hough lines, was used in this research to correlate those feature points. Since the parameter space is limited to two degrees and a few feature points, the computational load was greatly reduced to allow real-time application. Then the bounded lines marking the blade area were generated by searching the feature points along the Hough lines.

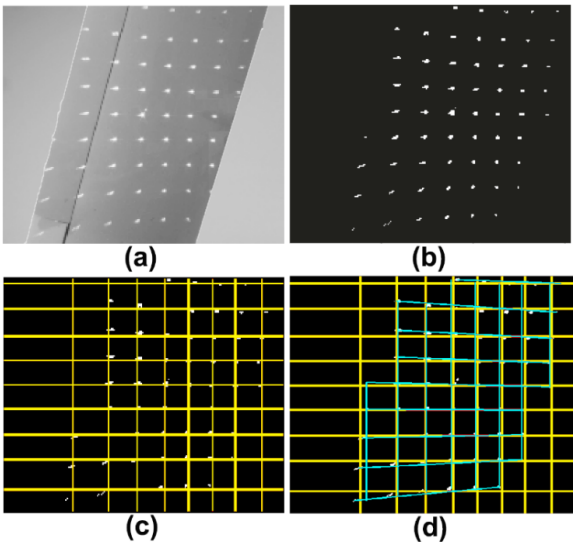

Figure. 5 Segmenting the WTB: (a) the grayscale image of the WTB with light pattern projection on; (b) the feature points; (c) Hough line matrix; (d) Bounded line of the WTB.

(2) Acquiring the initial disparity map.

The epipolar constraint, the uniqueness constraint, the ordering constraint were applied simultaneously to acquire the initial disparity map. According to the continuity constraint, search for the extreme disparity values in the blade area segmented in the previous step to obtain the current disparity range [Dmin, Dmax].

(3) Obtaining the PDH of the disparity matrix.

The PHD of the disparity matrix was generated by dividing the range of disparity values into 20 equal intervals and computing the probability distribution of each disparity interval. Only the disparity values of the matching points in the blade area segmented in step (i) were used in the statistic. An example of the PHD of a disparity matrix is depicted as below.

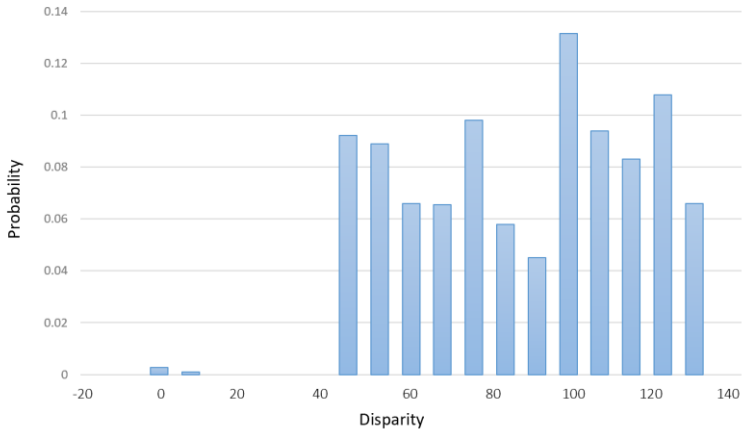

Figure. 6 An example of the PDH of a disparity matrix.

(4) Removing the discontinuous disparity.

A probability value between the maximum interval of discontinuous disparity interval and minimum probability of continuous disparity interval was selected, and then the disparity value corresponding to this probability was determined to be the threshold disparity Dt. All of the disparities less than Dt was removed from the PDH so that the disparity range was truncated to [Dt, Dmax].

(5) Optimizing the disparity map.

The removed disparities from the abobe step were then replaced with interpolated values. A

July – August 2020
ISSN: 0193-4120 Page No. 3608 - 3615

interpolated disparity value was determined by the mean of the disparity values of its eight nearest-neighbor points. In this way, those false disparities such as zero value disparities were eliminated.

5. Experimental setup

The experimental instruments include two daheng-image® CrashCam mini 3525 high-speed cameras, one 3D PRO laser Mini Green from prophotonix, and one PC equipped with an intel i9-9980HK 8-core cpu, 32GB memory, and a nVIDIA Quadro RTX 5000 GPU with 16GB VRAM. The CrashCam mini 3525 has a frame rate of 2,200fps under the resolution of 2560x1440. A VSTASV80-2MW wind turbine with a blade length of 39m was selected as a test target. The target wind turbine has three known deformations on its WTBs.

Figure. 7 The active stereovision system.

The active stereovision system was connected to the computer and was placed 3 meters in front of the WTB. In order to gain an ideal image quality, a pair of 8.5mm fixed focal length lens with a aperture of f/1.3-f/16 was installed onto the two CrashCam mini cameras. The estimated field view after the installation of the lens is 3100×2330mm at a focal length of 3 meters, which can cover the most of a WTB. The exposure time was set to 46μs in this experiment to capture clear images during the rotation of the target WTB.

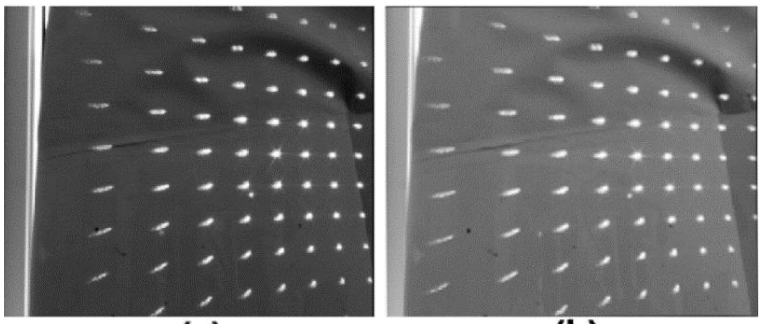

Figure. 8 The grayscale image pair of the rotating WTB captured with exposure time set at 46μs.

The deformations formed on the surface of WTBs usually contain abrupt shape changes due to the material properties. In this work, surface fitting was applied to process the cloud points obtained to determine the reference plane. The deformed surface was obtained via triangulation of the fitted 3D point clouds. Then the proposed active stereovision method was adopted to reconstruct the relative deformation depth to the reference plane and the width of the deformed area for each deformation area on the WTB.

TEST Engineering & Management

July – August 2020
ISSN: 0193-4120 Page No. 3608 - 3615

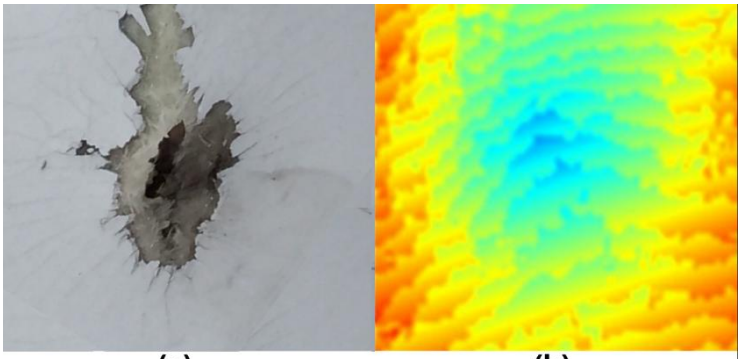

Figure. 9 One of the deformation areas on the target WTB and its disparity map.

The point clouds derived from the deformation areas appear to have abrupt depth changes compared to neighboring areas on the reference plane. The width and depth of these point clouds were measured using the proposed active stereovision method and the results were then compared with the measurements by vernier caliper. The coimparison indicates that the absolute percentage errors of the measurement results by the proposed method are within 11% of the measurement results by vernier caliper. The measurement results of the width of the deforamtions by the proposed method is more accurate than those of the depth of the deformations.

Table 1 Measurement results of the width and depth of the three deformations on the target WTB by active stereovision (mm)

Deformation number	Width			Depth		
	Active stereovision	Vernier caliper	Absolute percentage error	Active stereovision	Vernier caliper	Absolute percentage error
1	77.15	74.83	3.1%	4.01	3.80	5.50%
2	85.67	83.16	3.01%	9.33	8.84	5.54%
3	83.53	80.91	3.23%	8.76	7.89	11.02%

In the experiment period of time, the target WTB was rotating at a speed of 30 to 40 rotations per minute. Under this dynamic condition, the proposed method can capture clear image pairs and calculate the deformation width and depth in time. The main process and the corresponding delays are listed as below:

Table 2 Approximate delays for the main processing steps of the proposed method

Processing step	Approximate delay (seconds)
Grayscale conversion	0.04
Stereo matching	0.12
Disparity optimization	0.08
3D points reconstruction	0.03
Deformation measurement	0.01
Estimated total processing delay	0.32

6. Conclusion

To address the problem that the conventional method only measures the deformations on WTBs in a offline status, a real-time deformation detection method based on active stereovision is proposed in this paper which uses actively projected light patterns and high-speed cameras to improve the measurement performance, especially when the target WTB is in motion. Owing to the relative slow rotation speed of the WTB, high-speed cameras with appropriate exposure time can capture clear turbine blade pictures in the operational status. This method chooses laser as the active light source to adapt the strong outdoor ambient lighting condition confronting most wind turbines. The active projection of light patterns also contribute to an easier and faster stereo matching, as well as the removal of the WTB background image. To further improve the speed of stereo matching, the fast SAD criterion with the area matching window size 13×13 is adopted. WTB segmentation together with 5 constraints are combined in the process of disparity map optimization. The 3D reconstruction and surface fitting are then performed to determine and measure the deformation areas on the target WTB. The experiment results indicate that the proposed

July – August 2020
ISSN: 0193-4120 Page No. 3608 - 3615

method is efficient and reliable for the real-time detection and measurement of deformations on WTBs.

Acknowledgments

The author acknowledges the Fujian provincial educational department fund (Grant: JT180404), the Guiding Project of Natural Science Foundation of Fujian Province (Grant: 2019H0027)

References

[1] Wekesa D W, Wang C, Wei Y, et al. Experimental and numerical study of turbulence effect on aerodynamic performance of a small-scale vertical axis wind turbine. Journal of Wind Engineering and Industrial Aerodynamics. 157 (2016) 1-14.
[2] Pourazarm P, Caracoglia L, Lackner M, et al. Stochastic analysis of flow-induced dynamic instabilities of wind turbine blades. Journal of Wind Engineering and Industrial Aerodynamics. 137 (2015) 37-45.
[3] Qiao W, Lu D. A survey on wind turbine condition monitoring and fault diagnosis—Part I: Components and subsystems. IEEE Transactions on Industrial Electronics. 62(10) 2015 6536-6545.
[4] Qiao W, Lu D. A survey on wind turbine condition monitoring and fault diagnosis—Part II: Signals and signal processing methods. IEEE Transactions on Industrial Electronics. 62(10) 2015 6546-6557.
[5] Zeng J, Song B. Research on experiment and numerical simulation of ultrasonic de-icing for wind turbine blades. Renewable Energy. 113 2017 706-712.
[6] Skrimpas G A, Kleani K, Mijatovic N, et al. Detection of icing on wind turbine blades by means of vibration and power curve analysis. Wind Energy. 19(10) 2016 1819-1832.
[7] Habibi H, Cheng L, Zheng H, et al. A dual de-icing system for wind turbine blades combining high-power ultrasonic guided waves and low-frequency forced vibrations. Renewable Energy. 83 2015 859-870.
[8] Zhang C, Chen H P, Huang T L. Fatigue damage assessment of wind turbine composite blades using corrected blade element momentum theory. Measurement. 129 2018 102-111.
[9] Yang R, He Y, Zhang H. Progress and trends in nondestructive testing and evaluation for wind turbine composite blade. Renewable and Sustainable Energy Reviews. 60 2016 1225-1250.
[10] Sarrafi A, Mao Z, Niezrecki C, et al. Vibration-based damage detection in wind turbine blades using Phase-based Motion Estimation and motion magnification. Journal of Sound and Vibration. 421 2018 300-318.
[11] Coscetta A, Minardo A, Olivares L, et al. Wind turbine blade monitoring with Brillouin-based fiber-optic sensors. Journal of Sensors. 2017 1-5.
[12] Wang L, Zhang Z. Automatic detection of wind turbine blade surface cracks based on UAV-taken images. IEEE Transactions on Industrial Electronics. 64(9) 2017 7293-7303.
[13] Gómez Muñoz C, García Márquez F. A new fault location approach for acoustic emission techniques in wind turbines. Energies. 9(1) 2016 40.
[14] Muñoz C Q G, Márquez F P G, Tomás J M S. Ice detection using thermal infrared radiometry on wind turbine blades. Measurement. 93 2016 157-163.
[15] Li D, Ho S C M, Song G, et al. A review of damage detection methods for wind turbine blades. Smart Materials and Structures. 24(3) 2015 033001.
[16] Zhang S. High-speed 3D shape measurement with structured light methods: A review. Optics and Lasers in Engineering. 106 2018 119-131.
[17] Zhou H F, Dou H Y, Qin L Z, et al. A review of full-scale structural testing of wind turbine blades. Renewable and Sustainable Energy Reviews. 33 2014 177-187.
[18] Zhang Z. A flexible new technique for camera calibration. IEEE Transactions on pattern analysis and machine intelligence. 2000 22.
[19] Tippetts B J, Lee D J, Archibald J K, et al. Dense disparity real-time stereo vision algorithm for resource-limited systems. IEEE Transactions on Circuits and Systems for Video Technology. 21(10) 2011 1547-1555.
[20] Hirschmuller H, Scharstein D. Evaluation of stereo matching costs on images with radiometric differences. IEEE transactions on pattern analysis and machine intelligence. 31(9) 2008 1582-1599.
[21] Satoh S. Simple low-dimensional features approximating NCC-based image matching. Pattern Recognition Letters. 32(14) 2011 1902-1911.
[22] Hamzah R A, Ibrahim H. Literature survey on stereo vision disparity map algorithms. Journal of Sensors, 2016 1-23.